On the Mechanism of the Spin-Nonconserving Chemical Reaction $O(^3P) + HCCH \rightarrow CH_2(\tilde{a}^1A_1) + CO(X^1\Sigma^+)$. I. Feasibility

David R. Yarkony

Department of Chemistry, The Johns Hopkins University, Baltimore, Maryland 21218

Received: March 19, 1998; In Final Form: April 30, 1998

The mechanism of spin-forbidden reaction $O(^3P) + HCCH(\tilde{X}^1\Sigma_g^+) \rightarrow HCCHO(1,2^3A) \rightarrow HCCHO(^1A) \rightarrow CH_2(\tilde{a}^1A_1) + CO(X^1\Sigma_g^+)$ is discussed. Portions of the $^3A''-^1A'$, $^3A'-^1A'$, and $^3A''-^3A'$ surfaces of intersection and the spin−orbit coupling matrix elements are determined. An intermediate complex driven model is proposed. Intersystem crossing is expected to occur over the entire region between the intermediate complex, ^3HCCHO, and the transition state for the spin-allowed rearrangement, $^3HCCHO \rightarrow {}^3H_2CCO$. The barrier for the reaction arises from the formation of the adduct ^3HCCHO and is thus the same as that of the spin-allowed process forming $CH_2(\tilde{X}^3B_1)$.

I. Introduction

In a spin-nonconserving, spin-forbidden, chemical reaction, the total electronic spin angular momentum differs in the reactants and the products. In polyatomic molecules comprised exclusively of light atoms, these processes can be quite efficient despite the necessarily weak spin−orbit coupling. The efficiency is derived from repeated access to the crossing regions, regions of nuclear coordinate space where the nonrelativistic Born−Oppenheimer potential energy surfaces in question intersect. The archetypical example of this situation is spin-forbidden radiationless decay of a bound state. Here, molecular vibration results in repeated access to a crossing region leading to intersystem crossing and predissociation.[1] A generalization of this mechanism is responsible for intermediate complex driven reactions,[2−4] a class of spin-forbidden bimolecular reactions. In these reactions, intermolecular translation-to-vibration and intramolecular vibration-to-vibration energy transfer involving the reacting moieties results in formation of a metastable complex—the analogue of the bound state—that subsequently undergoes spin-forbidden predissociation, that is intersystem crossing to the product state. The location of the region or regions of nuclear coordinate space where the intersystem crossing occurs is key to understanding a reaction of this type. In this regard, it is important to note that nuclear motion proceeds on the reactant potential energy surface (or surfaces) until a crossing region is repeatedly encountered. Thus, it is not sufficient to consider only the energetics of the crossing regions, rather the relation to the dynamics on the reactant potential energy surface(s) must be considered.

There has been considerable interest[5−8] in the reaction of $O(^3P)$ with acetylene (H−C≡C−H) and with higher alkynes. These reactions have important implications for combustion chemistry.[9] In the case of acetylene, the principal products of this reaction are $CO + CH_2$ and $HCCO + H$. The $CO + CH_2$ products are obtained from a hydrogen shift following initial formation of an intermediate triplet ketocarbene complex, ^3HCCHO. The existence of the long-lived ketocarbene complex is evinced by the forward−backward symmetry in the center of mass product distributions reported in crossed molecular beam studies.[6] In the reactions of $O(^3P)$ with heavier alkynes, when $CO(X^1\Sigma^+)$ is formed, a singlet carbene is the companion product. From this result, it was concluded[8] that for the heavier alkynes the triplet ketocarbene undergoes intersystem crossing to a singlet moiety which subsequently decomposes to $CO(X^1\Sigma^+)$ and a singlet carbene. However, experimental difficulties precluded direct identification of the carbene formed in the acetylene case.[8]

This work therefore considers the possibility of the analogous reaction for acetylene:

$$O(^3P) + HCCH(\tilde{X}^1\Sigma_g^+) \rightarrow CH_2(\tilde{a}^1A_1) + CO(X^1\Sigma_g^+) \quad (1a)$$

focusing principally on the intersystem crossing, the event represented within the square brackets in the reaction sequence

$$O(^3P) + HCCH(X^1\Sigma_g^+) \rightarrow [HCCHO(^3A'',{}^3A') \rightarrow HCCHO(^1A')] \rightarrow CH_2(\tilde{a}^1A_1) + CO(X^1\Sigma_g^+) \quad (1b)$$

where C_s symmetry designations have been used for simplicity, since the ground $^3A''$, and first excited $^3A'$, electronic states of the ketocarbene ^3HCCHO are planar.[5] The assumption of planarity will be relaxed in this work since it is also known that the transition state for the rearrangement $^3HCCHO \rightarrow$ triplet ketene (^3H_2CCO) is nonplanar.[5]

The present analysis will be guided by the mechanism suggested by Figure 1, which summarizes the known[5] energetics relevant to reaction 1. It benefits considerably from a previous study of the spin-conserving pathways for the reaction of $O(^3P)$ with $HCCH(\tilde{X}^1\Sigma_g^+)$ by Harding and Wagner[5] (denoted HW below) and also the abundant theoretical work on ketene. See, for example, refs 10 and 11 and references contained therein. The existence of a deep well corresponding to the ground $\tilde{X}^1A_1$ state of ketene suggests that low-energy singlet−triplet intersections may exist in the shaded region. This region would be accessed when intermode energy transfer produces the long-lived intermediate ketocarbene complexes, HCCHO-($^3A''$ and $^3A'$ or 1^3A and 2^3A). Following the intersystem

S1089-5639(98)01568-0 CCC: $15.00
Published on Web 06/12/1998

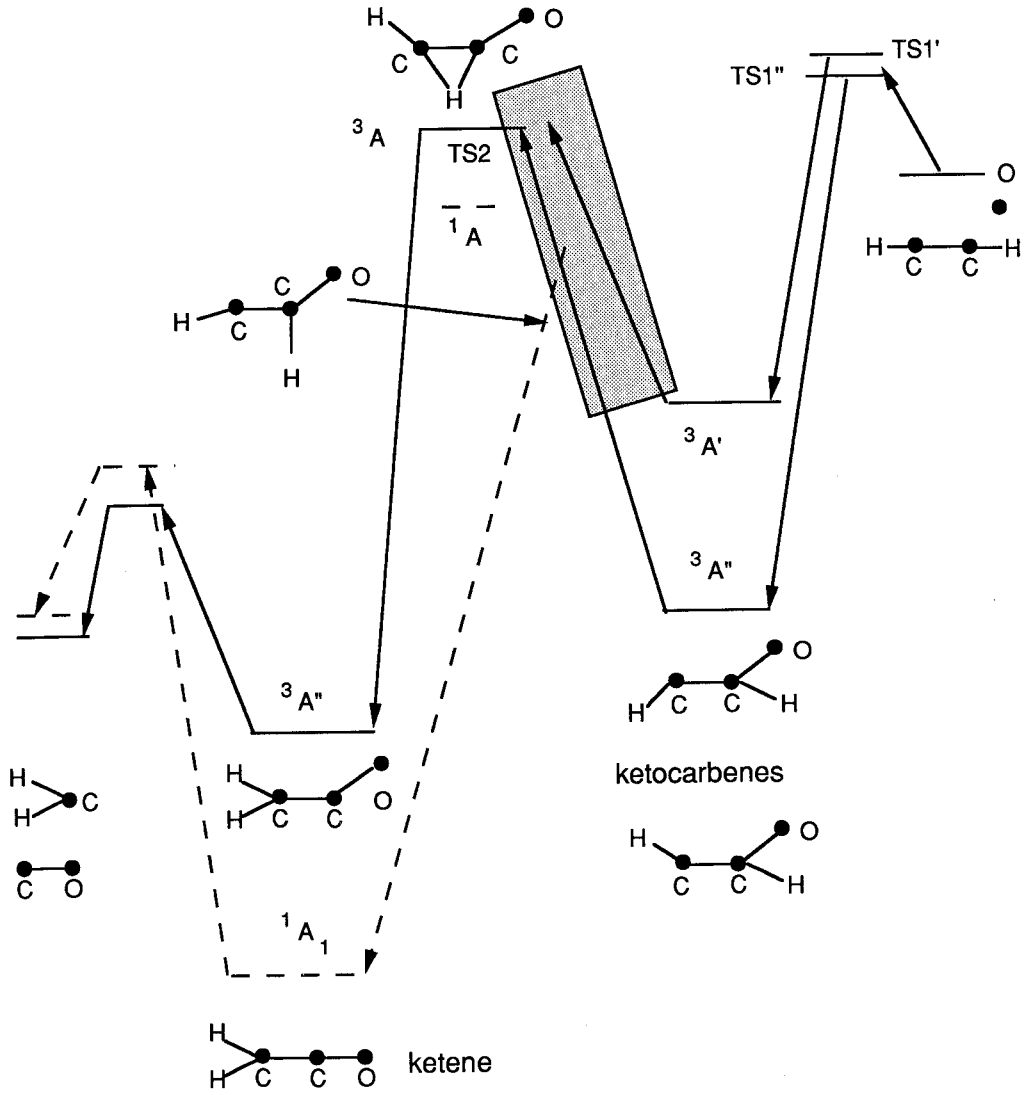

Figure 1. Schematic representation of reaction 1b based on refs 5 and 10. The shaded region is the crossing region suggested by ref 8.

crossing, the system could evolve along a potentially barrierless[12] path to $H_2CCO(\tilde{X}^1A_1)$ and subsequently to products.

Section II discusses the state-averaged multiconfigurational self-consistent field(SA-MCSCF)/configuration interaction (CI) wave functions[13] used to describe the states in question and the spin−orbit interactions that drive the intersystem crossing. Section III describes the results of the present calculations, and section IV summarizes and concludes this paper.

II. Theoretical Approach

Of the three triplet states arising from $O(^3P)$, two lead to bound triplet states, the $^3A''$ and $^3A'$ or 1^3A and 2^3A states, in the ketocarbene, ^{3}HCCHO, region, while for the product channel, the singlet state is nondegenerate and totally symmetric. At sufficiently high temperatures, paths to both the $^3A''$ and $^3A'$ states of ^{3}HCCHO are accessible.[5] Once formed, the electronically excited $^3A'$ state can undergo internal conversion to the $^3A''$ state, intersystem cross to the $^1A'$ state, or be quenched collisionally to the $^3A''$ state. Therefore, in this work, we focus on the $^3A''$, $^3A'$, and $^1A'$ electronic states and three nonadiabatic pathways: $^3A''-{}^1A'$ intersystem crossing; $^3A'-{}^1A'$ intersystem crossing; and $^3A'-{}^3A''$ internal conversion followed by $^3A''-{}^1A'$ intersystem crossing. The $^3A'-{}^3A''$ internal conversion is also relevant to the spin-allowed pathway discussed by HW. This choice of electronic states reflects the preeminent role of planar structures in the ketocarbene region, as well as the symmetry of the ground singlet state of ketene and of the singlet products. However, additional mechanistic pathways may be possible involving the $^1A''$ state. Intersystem crossing to this state could produce $H_2CCO(\tilde{X}^1A_1)$ via an internal conversion or directly, if it is the lowest singlet state, by accessing nonplanar geometries.[12] The possibility of contributions from these additional pathways will be subject of future studies.

A. Electronic Structure Treatment. The electronic structure calculations reported in this work were carried out in either C_s symmetry, for the $^3A''$, $^3A'$, and $^1A'$ states, or C_1 symmetry, for the $1,2^3A$ and ^1A states. The wave functions were obtained at the SA-MCSCF/second-order configuration interaction (SOCI) level of theory. The SOCI expansions—all configuration state functions (CSFs)[14] arising from zero, one, and two electron excitations from the active orbitals to all the virtual orbitals—employed the following partitioning of the molecular orbitals in C_s symmetry: $[1a'\text{-}4a']^8$ $\{5a'\text{-}10a', 1a''\text{-}2a''\}$.[14] Here, the square brackets denote the core orbitals, the 1s orbitals of carbon and oxygen and the 2s orbital on oxygen, kept fully occupied in the SOCI expansion, the curly brackets denote the active orbitals, and the superscripts indicate the number of electrons in the corresponding molecular orbital set. The $9a'$, $10a'$ and the $1a''$, $2a''$ molecular orbitals, represented qualitatively as

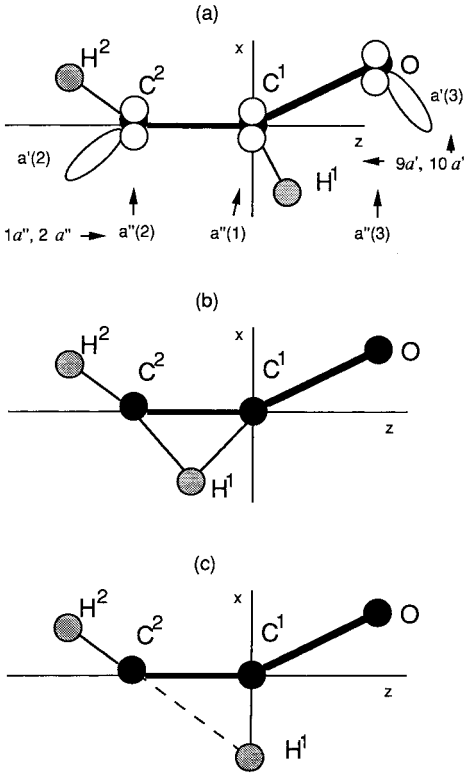

Figure 2. Atomic labeling conventions used in this study. Also indicated are atom centered, planar orbitals, a′(*i*), $i = 1, 2$, which contribute to the 9*a*′ and 10*a*′ molecular orbitals and the out-of-plane p_π orbitals, a″(*i*), $i = 1-3$, which contribute to the 1*a*″ and 2*a*″ molecular orbitals. (a) *trans*−HCCHO, (b) TS2, and (c) intermediate region $\angle C^2C^1H = 90°$.

linear combinations of the atom-centered σ and π functions, respectively, in Figure 2a, will be of particular concern.

The molecular orbitals were determined from a complete active space[15−17] SA-MCSCF procedure in which one $^3A''$ state, one $^3A'$ state, and one $^1A'$ state were averaged with equal weights. The weights were 0.51, 0.49, and 0.5 for the $1,2^3A$ and ^1A states in the C_1 symmetry calculations. To facilitate convergence of the SA-MCSCF procedure the core and active spaces were redefined, for the orbital optimizations only, as [1*a*′-7*a*′][14] {8*a*′-10*a*′, 1*a*″-2*a*″}.[8] While this three state averaging is convenient, and certainly adequate for this initial treatment as shown below, for reasons noted subsequently, alternative approaches will be considered a future work which will refine the energetics presented here using larger atomic orbital bases.

All the calculations reported in this work, including the spin−orbit calculations which use full Breit−Pauli form[1] of the spin−orbit operator, and the geometry searches—determination of (constrained) minima on the singlet and triplet surfaces, and surface intersection points—employed standard Dunning−Huzinaga double-ζ plus polarization (DZP) basis[18] sets, C[9s5p1d]/(4s2p1d), O[9s5p1d]/(4s2p1d), and H[4s1p]/(2s1p). On the basis of the above partitioning of the molecular orbitals, this basis set yielded SOCI expansions comprised of 536 780, 538 420, and 336 176 CSFs for the $^3A''$, $^3A'$, and $^1A'$ states, and 1 075 200 and 666 450 CSFs for the $1,2^3A$ and ^1A states, respectively. All points on surfaces of intersection were determined using an analytic gradient-driven algorithm reported previously[19] and are degenerate to <1 cm^{-1} at the SOCI level.

B. Spin−Orbit Interactions. In the absence of spatial symmetry, there are three independent matrix elements of the spin−orbit operator between the singlet state

$$\Psi(^1A) = \Psi[^1A(0)] \tag{2a}$$

and the triplet states

$$\Psi_{I,1}(^3A) = i\Psi[I^3A(0)] \tag{2b}$$

$$\Psi_{I,2}(^3A) = i\{\Psi[I^3A(1)] - \Psi[I^3A(-1)]\}/\sqrt{2} \tag{2c}$$

$$\Psi_{I,3}(^3A) = \{\Psi[I^3A(1)] + \Psi[I^3A(-1)]\}/\sqrt{2} \tag{2d}$$

where in the term symbol $^{2S+1}X(M_S)$, M_S denotes the *z*-component of the total electron spin *S*, the geometry dependence has been suppressed to avoid excessive subscripting, and a time-reversed electronic basis has been used so that all matrix elements will be real valued.[20,21] In this representation, spin−orbit matrix elements are

$$H_z^{so}(I^3A) \equiv \langle\Psi_{I,1}(^3A)|H^{so}|\Psi(^1A)\rangle \tag{3a}$$

$$H_x^{so}(I^3A) \equiv \langle\Psi_{I,2}(^3A)|H^{so}|\Psi(^1A)\rangle \tag{3b}$$

$$H_y^{so}(I^3A) \equiv \langle\Psi_{I,3}(^3A)|H^{so}|\Psi(^1A)\rangle \tag{3c}$$

When C_s symmetry is used the coordinate system is chosen such that the *xz*-plane is the C_s plane. Then for $I^3A = {}^3A''$, there are only two independent nonzero interstate matrix elements since $H_y^{so}(^3A'') = 0$, while for $I^3A = {}^3A'$ $H_x^{so}(^3A') = 0$ and $H_z^{so}(^3A') = 0$. These relationships are easily deduced from the observation that

$$\sigma_{xz}\{\Psi[^3A(1)] \pm \Psi[^3A(-1)]\} = \pm\chi(A)\{\Psi[^3A(1)] \pm \Psi[^3A(-1)]\} \tag{4a}$$

$$\sigma_{xz}\,\Psi[^{2S+1}A(0)] = (-1)^S\chi(A)\,\Psi[^{2S+1}A(0)] \tag{4b}$$

where σ_{xz} is operator for a reflection in the *xz*-plane, $\chi(A') = 1$ and $\chi(A'') = -1$. In this case for $I^3A = {}^3A'$, $H_y^{so}(^3A')$ is independent of the orientation of the molecule in the *xz*-plane, otherwise $H_x^{so}(I^3A)$, $H_y^{so}(I^3A)$, and $H_z^{so}(I^3A)$ are orientation dependent. For this reason, only $H^{so}(I^3A)$, where $H^{so}(I^3A)^2 \equiv H_x^{so}(I^3A)^2 + H_y^{so}(I^3A)^2 + H_z^{so}(I^3A)^2$ will be reported.

III. Results and Discussion

In this work, all energies will be expressed in kilocalories per mole relative to $E_{3A''} = -151.916\,228$ au, the energy at the $O(^3P)$ + HCCH asymptote with R(C−C) = 2.273 a_0 and R(C−H) = 2.005 a_0. At this geometry, $E_{3A'} = -151.916\,213$ au so that there is negligible ($\sim$3.2 cm^{-1}) splitting of the $O(^3P)$ asymptotically. From $E_{1A'}$, the $O(^1D)-O(^3P)$ separation is 17 495(15 876) cm^{-1} which is typical for the DZP basis and in satisfactory accord with the experimental value[22] given parenthetically. This level of treatment yields an equilibrium structure for $H_2CCO(\tilde{X}^1A_1)$, $\mathbf{R}_{eqK1}$, Table 1, in good accord with a recent high level ab initio treatment.[23] $E_{1A'}(\mathbf{R}_{eqK1}) = -118(-120.8)$ kcal/mol is in satisfactory accord with the SDCI + QC value inferred from HW, given parenthetically, but somewhat higher than the inferred best value estimate of HW $E_{1A'}(\mathbf{R}_{eqK1}) = -133$ kcal/mol. The inferred $E_{1A'}(\mathbf{R}_{eqK1})$s are obtained from the SDCI + QC value of $E_{3A''}(\mathbf{R}_{eqK3}) = -66.1$ kcal/mol, and the best estimate of $E_{3A''}(\mathbf{R}_{eqK3}) = -78.9$ kcal/mol, both from HW together with $T_e[H_2CCO(\tilde{a}^3A'')] = 19\,150$ cm^{-1} from ref 10. Here, $\mathbf{R}_{eqK3}$ is the equilibrium geometry of $H_2CCO(\tilde{a}^3A'')$.

TABLE 1: Planar Structures[a]

R(C^1O)	R(CC)	R(C^2H^2)	R(C^1H^1)	∠CCO	∠H^2CC	∠CCH^1	$E_{^3A''}$	$H^{so}(^3A'')$	$E_{^3A'}$	$H^{so}(^3A')$
					$^1A'$					
					$^1A_1$ H_2CCO[c]					
2.201	2.500	2.040		179.6	119.1					
2.203[c]	2.492	2.037		180	121.9					
					$^3A''$					
					(1) $^3A''$ *trans*−HCCHO					
2.343	2.661	2.052	2.072	117.7	127.0	120.3	−49.3			
2.336[b]	2.739	2.049	2.078	121.6	129.8	116.9	−49.2			
					(2a) $^3A''$−$^1A'$ *trans*−HCCHO					
2.329	2.927	2.110	2.080	124.6	96.5	117.0	−28.3	18.1		
					(2b) $^3A''$−$^1A'$ *trans*−HCCHO, R(C^1−C^2) = 2.75					
2.340	2.75	2.123	2.086	128.2	92.8	116.7	−24.7	20.6		
					(2c) $^3A''$−$^1A'$ *trans*−HCCHO, R(C^1−C^2) = 2.65					
2.339	2.65	2.140	2.091	131.4	88.9	116.2	−18.4	15.0		
					(3) $^3A''$ *cis*−HCCHO					
2.338	2.648	2.050	2.090	124.5	131.2	115.2	−45.8			
					(4) $^3A''$−$^1A'$ *cis*−HCCHO					
2.377	2.514	2.036	2.106	148.5	134.2	104.8	−28.8	35.0		
					(5a) $^3A''$−$^1A'$ *cis*−HCCHO, ∠$C^2C^1H^1$ = 90°					
2.297	2.627	2.028	2.141	140.8	173.0	90.0	−27.3	3.8		
					(5b) $^3A''$−$^1A'$ *trans*−HCCHO, ∠$C^2C^1H^1$ = 90°, R(CC) = 2.42					
2.346	2.420	2.033	2.180	150.3	158.7	90.0	−16.7	27.8		
					(6) $^3A''$ *trans*−HCHCO, R(C^1H^1) = R(C^2H^1) = 2.6					
2.266	2.636	2.075	2.600	149.8	138.3	59.5	6.0			
					(7) $^3A''$−$^1A'$ *trans*−HCHCO, R(C^1H^1) = R(C^2H^1) = 2.6					
2.253	2.793	2.075	2.600	138.1	137.4	57.5	12.0	5.11		
					$^3A'$					
					(8) $^3A'$ *trans*−HCCHO					
2.545	2.495	2.037	2.071	130.0	138.8	121.1			−26.6	
2.574[b]	2.483	2.038	2.062	129.7	140.4	121.5			−24.4	
					(9) $^3A'$−$^1A'$ *trans*−HCCHO					
2.545	2.497	2.038	2.069	129.2	138.5	121.5			−26.5	9.73
					(10) $^3A'$ *cis*−HCCHO					
2.538	2.499	2.036	2.073	126.2	134.4	123.2			−27.3	
					(11) $^3A'$−$^1A'$ *cis*−HCCHO					
2.511	2.515	2.044	2.072	132.4	133.9	121.3			−26.1	6.46
					(12) $^3A'$ *trans*−HCHCO, R(C^1H^1) = R(C^2H^1) = 2.4					
2.527	2.470	2.036	2.40	132.3	157.4	59.0			32.0	
					(13) $^3A'$−$^1A'$ *trans*−HCHCO, R(C^1H^1) = R(C^2H^1) = 2.4					
2.619	2.484	2.033	2.40	112.3	163.7	58.8			39.0	
					(14) $^3A'$−$^1A'$ *cis*−HCCHO, ∠$C^2C^1H^1$ = 90°					
2.551	2.508	2.030	2.077	123.1	136.0	90.0			−2.3	8.9
					$^3A''$−$^3A'$					
					(15a) $^3A''$−$^3A'$ *trans*−HCCHO					
2.558	2.440	2.030	2.116	140.8	140.5	126.5	−20.8		−20.8	
					(15b) $^3A''$−$^3A'$ *trans*−HCCHO, R(C− O) = 2.65					
2.650	2.438	2.029	2.105	139.6	141.7	127.2	−20.3		−20.3	
					(15c) $^3A''$−$^3A'$ *trans*−HCCHO, R(C− O) = 2.85					
2.850	2.435	2.029	2.085	136.9	143.9	129.6	−14.9		−14.9	
					(15d) $^3A''$−$^3A'$ *trans*−HCCHO, R(C− O) = 3.0					
3.00	2.428	2.028	2.075	135.3	146.4	131.5	−8.70		−8.70	
					(15e) $^3A''$−$^3A'$ *trans*−HCCHO, R(C− O) = 3.25					
3.25	2.406	2.023	2.063	133.0	152.5	135.5	3.86		3.86	

[a] All structures are minima on the indicated potential energy surface or surface of intersection with indicated constraints if any. Distances in a_0, angles in degrees, H^{so} in cm^{-1}. Energies in kcal/mol relative to $E_{^3A''}$ = −151.916 227 9 au the energy of O(^{3}P) + HCCH with R(C−C) = 2.273 a_0, R(C−H) = 2.005 a_0. [b] From ref 5 at SDCI + QC level. [c] $E_{^1A_1}$ = −118.8 kcal/mol. Results from ref 23 below those of present work.

Table 1 reports the equilibrium structures of four ketocarbenes, $^3A''$, $^3A'$−*cis*-HCCHO and $^3A''$, $^3A'$−*trans*-HCCHO, points *1*, *3*, *8*, and *10* (see Figure 2a). The $^3A''$($^3A'$) structures are stable by ∼47(∼27) kcal/mol with respect to the HCCH + O(^{3}P) asymptote. The geometries and energetics are in good accord with the previous results of HW obtained at the SDCI + QC level.[5] See Table 1 points *1* and *8*.

The above comparisons support the reliability of the current approach.

R(C^1−O) and R(C−C) for points *1*, *3*, *8*, and *10* in Table 1 evince the 1,3-biradical character of HCCHO($^3A'$) and the carbene character of HCCHO($^3A''$) pictured in Figure 3 (see also HW). The 1, 3-biradical corresponds to the electron configuration $C_I[^3A'] \equiv ...9a'10a'1a''^2 2a''^2$ with $9a' \approx a'(3)$,

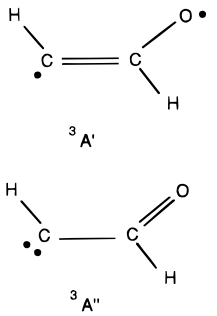

Figure 3. 1,3−Biradical and carbene structures characteristic of ^{3}A′ and ^{3}A″ states at their equilibrium geometries.

$10a' \approx a'(2)$, $1a'' \approx a''(1) + a''(2)$, and $2a'' \approx a''(3)$. The carbene corresponds to the electron configuration $C_I[^3A''] \equiv ...9a'^2 10a' 1a'' 2a''$ with the a' orbitals as above, $1a'' \approx a''(1) + a''(3)$ and $2a'' \approx a''(2)$, although as noted below the localized description of the $1a''$ and $2a''$ orbitals is somewhat simplistic. Here, the ellipsis denotes the $1-8a'$ doubly occupied orbitals. The atom-centered orbitals, a′(i) and a″(i), are pictured in Figure 2a. While the current SA-MCSCF/CI wave functions are clearly able to describe these diverse structures, this analysis indicates that a more flexible, and considerably more expensive, SA-MCSCF/CI procedure, including an additional a'' orbital in the active space, and/or separate treatments of the ^{3}A″ and ^{3}A′ states, would provide an enhanced description. This extension of the present approach will be used in a subsequent work to refine the energetics presented here.

The following subsections consider intersystem crossing and internal conversion in three connected regions of nuclear coordinate space: the region of the ^{3}HCCHO complexes (labeled ketocarbenes in Figure 1), the region of the transition state for the ^{3}HCCHO → ^{3}H$_2$CCO rearrangement (TS2 in Figure 1), and finally the intermediate region describing the migration of H[1] from ^{3}HCCHO structures to TS2 (the shaded region in Figure 1). Since the ^{3}A″−^{1}A′, ^{3}A′−^{1}A′, and ^{3}A″−^{3}A′ surfaces of intersection have dimension 6 in C_s symmetry, it is not practical to map out these surfaces of intersection. Instead, representative points are considered.

A. Internal Conversion in the Ketocarbene Region. Internal conversion of the 2^3A state to the 1^3A state is facilitated by conical intersections of the ^{3}A′ and ^{3}A″ potential energy surfaces, if they exist. For this reason, points on the ^{3}A″−^{3}A′ conical intersection seam were sought. Table 1 presents energy optimized points on this seam, points *15a*−*15e*. For point *15a*, the energy is minimized subject only to the requirement of degeneracy of the ^{3}A′ and ^{3}A″ states, whereas for points *15b*−*15e*, R(C^1−O) was also constrained to 2.65, 2.85, 3.0, and 3.25 a_0, respectively. Each of the conical intersection points is lower in energy than either the O(^{3}P) + HCCH asymptote or the transition state on ^{3}A′ potential energy surface for forming ^{3}HCCHO, TS1′ in Figure 1, for which R(C−O) ≈ 3.56 a_0.[5] Thus after overcoming the barrier on the 2^3A(^{3}A′) potential energy surface, the system can undergo internal conversion, through the ^{3}A″−^{3}A′ seam of conical intersections, to the 1^3A state. In a future work this point will be critically examined by considering the energetics on paths from TS1′ to these conical intersections, and the subsequent motion on the 1^3A potential energy surface.

B. Intersystem Crossing in the Ketocarbene Region. Using structures *1, 3, 8,* and *10* as starting points, (local) minimum energy points on the ^{3}A″−^{1}A′ and ^{3}A′−^{1}A′ surfaces of intersection were determined, points *2a, 4, 9,* and *11*. Each of these four minimum energy crossing points(MECPs) is approximately 27 ± 2 kcal/mol *below* the O(^{3}P) + HCCH asymptote. These energetics reflect an earlier result[12] that, for planar geometries in this region, the lowest singlet state is considerably higher than the lowest triplet state. For the ^{3}A″−^{1}A′ MECP near *trans*-HCCHO, point *2a*, R(C^1−C^2) is long so that it is germane to consider the effect of R(C^1−C^2) on the energy of the crossing point. This was accomplished by constraining R(C^1−C^2) to 2.75 and 2.65 a_0. The results, points *2b* and *2c*, are presented in Table 1. These structures are approximately 4 and 10 kcal/mol higher in energy than the structure obtained without the R(C−C) constraint, but still well below the O(^{3}P) + HCCH asymptote. R(C^1−C^2) = 2.65 a_0 is more representative of R(C^1−C^2) in the ketocarbene region and near TS2 as discussed below.

The *cis*- and *trans*-HCCHO ^{3}A′−^{1}A′ intersections, points *9* and *11*, are quite close to the corresponding ^{3}A′ minima, points *8* and *10* (which are approximately 20 kcal/mol above the ^{3}A″ minimum), Table 1. In this region, the ^{1}A′ state is constituted principally from either or both of the electron configurations $C_I[^1A'] \equiv ...9a'^2 10a'^2 1a''^2$ and $C_{II}[^1A'] \equiv ...9a' 10a' 1a''^2 2a''^2$. $C_{II}[^1A']$ represents a singlet 1,3-biradical. The proximity of the minimum on the ^{3}A′ surface and the MECP on the ^{3}A′−^{1}A′ surface of intersection is consistent with the 1,3-biradical structure of the ^{3}A′ state and the (partial) biradical structure of the ^{1}A′ state with unpaired electrons in the largely spatially distinct $9a'$and $10a'$ orbitals, Figure 2a and 3a. For points *9* and *11* $H^{so}(^3A')$ is small, ∼6−10 cm^{-1}. This is reasonable. The $C_I[^1A']$ contribution to $H^{so}(^3A')$ is expected to be small since it differs by a two electron excitation from $C_I[^3A']$ and the contribution arising from $C_{II}[^1A']$, $\sim\langle 9a'|h_{eff}^{so}|10a'\rangle$, involves the spatially disparate $9a'$ and $10a'$ orbitals. Here, h_{eff}^{so} is an effective one electron spin−orbit operator.[1]

$H^{so}(^3A'')$ is in general larger than $H^{so}(^3A')$ and exhibits a significant geometry dependence. This can be understood as follows. $C_I[^3A'']$ differs from $C_I[^1A']$ and $C_{II}[^1A']$ by the single electron promotions $2a'' \rightarrow 10a'$ and $9a' \rightarrow 2a''$, respectively, so that $H^{so}(^3A'') \approx |k_1(\mathbf{R})\langle 10a'|h_{eff}^{so}|2a''\rangle + k_2(\mathbf{R})\langle 9a'|h_{eff}^{so}|2a''\rangle|$. The $2a''$ orbital is not pure C−C π, a″(1) and a″(2), in character but acquires some oxygen, a″(3), character so that both $\langle 9a'|h_{eff}^{so}|2a''\rangle$ and $\langle 10a'|h_{eff}^{so}|2a''\rangle$ contribute to $H^{so}(^3A'')$. The changing character of the ^{1}A′ state, that is changes in the $k_i(\mathbf{R})$, together with the changes in oxygen character of the $2a''$ orbital produce the geometry dependence in $H^{so}(^3A'')$ evident in Table 1 points *2a*−*2c* and *4*.

C. The ^{3}HCCHO → ^{3}H$_2$CCO Transition-State (TS2) Region. HW have demonstrated that the transition state for ketocarbene−ketene interconversion on the lowest triplet surface (TS2) does not have C_s symmetry. However, the energy lowering from the C_s constrained transition state which occurs on the ^{3}A″ potential energy surface is only about 5 kcal/mol. For this reason, structures of the form $H^2C^2H^1C^1O$ (Figure 2b) were considered both with and without the constraint of C_s symmetry. Table 1 reports the ^{3}A″−^{1}A′ and ^{3}A′−^{1}A′ MECPs subject to the constraint R(C^2−H^1) = R(C^1−H^1) = β, with β optimized (in 0.1 a_0 steps) to minimize the energy at the point of intersection, points *7* and *13*. $E_{^3A'} = E_{^1A'}$ at the constrained ^{3}A′−^{1}A′ crossing, point *13*, is well above the HCCH + O(^{3}P) asymptote and is not considered further. At the ^{3}A″−^{1}A′ constrained crossing (point *7*, β = 2.6 a_0), $E_{^3A''} = E_{^1A'} = 12.0$ kcal/mol. However, minimizing only $E_{^3A''}$ with R(C^2−H^1) = R(C^1−H^1) = 2.6 a_0, point *6*, yields $E_{^3A''} = 6$ kcal/mol (see Table 1). Thus, it is unlikely that a trajectory *on* the ^{3}A″ surface will access this crossing.

TABLE 2: Nonplanar Structures[a]

	$C^{12}H$ (2.6)	$C^{12}H$ (2.4)	TS2[b]	CCH (90)[c]
$R(C^1\text{-}O)$	2.273	2.281	2.275	2.255
$R(C^2\text{-}C^1)$	2.751	2.717	2.636	2.660
$R(C^2\text{-}H^2)$	2.069	2.067	2.069	2.030
$R(C^1\text{-}H^1)$	2.600	2.400	2.467	2.168
$\angle C^2C^1O$	133.4	131.4	138.8	139.9
$\angle H^2C^2C^1$	136.9	137.2	137.3	166.3
$\angle C^2C^1H^1$	58.1	55.5	64.3	90.0
$\angle OC^2C^1H^1$	140.6	132.9	125.3	3.2
$\angle OC^2C^1H^2$	−3.5	−1.0	12.9	−5.9
$E(^3A)[E(^1A)]$	3.8	3.3	2.5[−10.3]	−26.9
$H^{so}(^3A)$	17.6	18.5	18.7	2.6

[a] Distances in a_0, angles in degrees, H^{so} in cm^{-1}. Energies in kcal/mol relative to $E_{^3A''} = -151.916\,227\,9$ au the energy of $O(^3P)$ + HCCH with R(C−C) = 2.273 a_0, R(C−H) = 2.005 a_0. [b] SDCI + QC results of ref 5 $R(C^1-O) = 2.314$ a_0, $R(C^1-C^2) = 2.636$ a_0, $R(C^2-H^2) = 2.066$ a_0, $R(C^1-H^1) = 2.489$ a_0, $\angle C^2C^1O = 138.4°$ $\angle H^2C^2C^1 = 135.9°$, $\angle C^2C^1H^1 = 65.6°$, $\angle OC^1C^2H^2 = 122.7°$, $\angle OC^1C^2H^1 = 12.0°$, $E_{^3A} = 3.30$ kcal/mol. [c] Representative point on nonplanar portion of surface of intersection near point 5a (degeneracy 3.7 cm^{-1}).

The situation changes dramatically when the constraint of C_s symmetry is relaxed. The MECPs with $R(C^2-H^1) = R(C^1-H^1) = \beta$, $\beta = 2.4$ and 2.6, but with the C_s constraint relaxed, denoted $C^{12}H(\beta)$, are reported in Table 2. $E_{1^3A} = E_{1^1A}$ is 3.8 and 3.3 kcal/mol, respectively, at these crossing points. The spin−orbit interaction, Table 2, is approximately 18 cm^{-1} in this region. Also given in Table 2 is the transition-state structure for the ^{3}HCCHO−$^3H_2$CCO interconversion, $\mathbf{R}_{TS2}$, which is in good accord with SDCI + QC result of HW (see Table 2). The energies at the $C^{12}H(\beta)$ crossings are close to $E_{13A}(\mathbf{R}_{TS2}) = +2.5$ kcal/mol, Table 2. Although these crossing points are reasonably close to the transition state, intersystem crossing in this region is improbable since repeated access to this region is unlikely.

$E_{^1A}(\mathbf{R}_{TS2}) = -10.3$ kcal/mol; that is 12.8 kcal/mol *below* the triplet state. This suggests the existence of additional singlet−triplet intersections near points on the reaction path *prior* to TS2. It is to this issue that we now turn.

D. Region between ^{3}HCCHO and TS2. The parameter $\angle C^2C^1H^1$ can be used as an approximate reaction coordinate to describe the ketocarbene−ketene rearrangement.[12] Here, we focus on the region with $\angle C^2C^1H^1 = 90°$, Figure 2c, which is between $\angle C^2C^1H^1 = 117°$, the ketocarbene region, and $\angle C^2C^1H^1 = 64°$ near TS2. With this constraint, the 1^3A-1^1A MECP was found to be approximately—see Table 2, point CCH(90)—planar. Table 1 reports three points in this region, points *5a*, *5b*, and *14*. Point *14*, on the $^3A'-{}^1A'$ surface of intersection is 2.3 kcal/mol below the $O(^3P)$ + HCCHO asymptote, whereas points *5a* and *5b* on the $^3A''-{}^1A'$ surface of intersection are stable by 27.3 and 16.7 kcal/mol relative to the $O(^3P)$ + HCCH asymptote. Analysis of the energy gradients on the $^3A''$ and $^1A'$ potential energy surfaces suggests that from points *5a* and *5b* the system will evolve: on the $^1A'$ potential energy surface, to $H_2CCO(\tilde{X}^1A_1)$, and on the $^3A''$ potential energy surface to ^{3}HCCHO. Figures 4a and 4b demonstrate that this is in fact the case. These figures report the geometry and energetics along the paths generated by following the gradients on the $^3A''$ and $^1A'$ potential energy surfaces. These gradient directed paths, which lead to $H_2CCO(\tilde{X}^1A_1)$ on the $^1A'$ potential energy surface and to *cis*-^{3}HCCHO (point *3*) on the $^3A''$ potential energy surface, show no (significant) barrier. The small oscillations in R(C−C) and R(C−O) in Figure 4a are attributable to the use of gradient directed paths rather than intrinsic reaction coordinate paths.[24] Similar outcomes on the $^3A''$ and $^1A'$ potential energy surfaces were obtained from point *5b*. This analysis evinces the key role played by this region in reaction 1.

An analysis of the energy gradients on the $^3A'$ and $^1A'$ potential energy surfaces indicates that a similar result would be obtained from point *14*. However, as noted above direct intersystem crossing from the $^3A'$ state may not occur.

In this region, the $^1A'$ state is dominated by the electron configuration $C_{III}[^1A'] \equiv ...9a'^2 1a''^2 2a''^2$. This closed shell

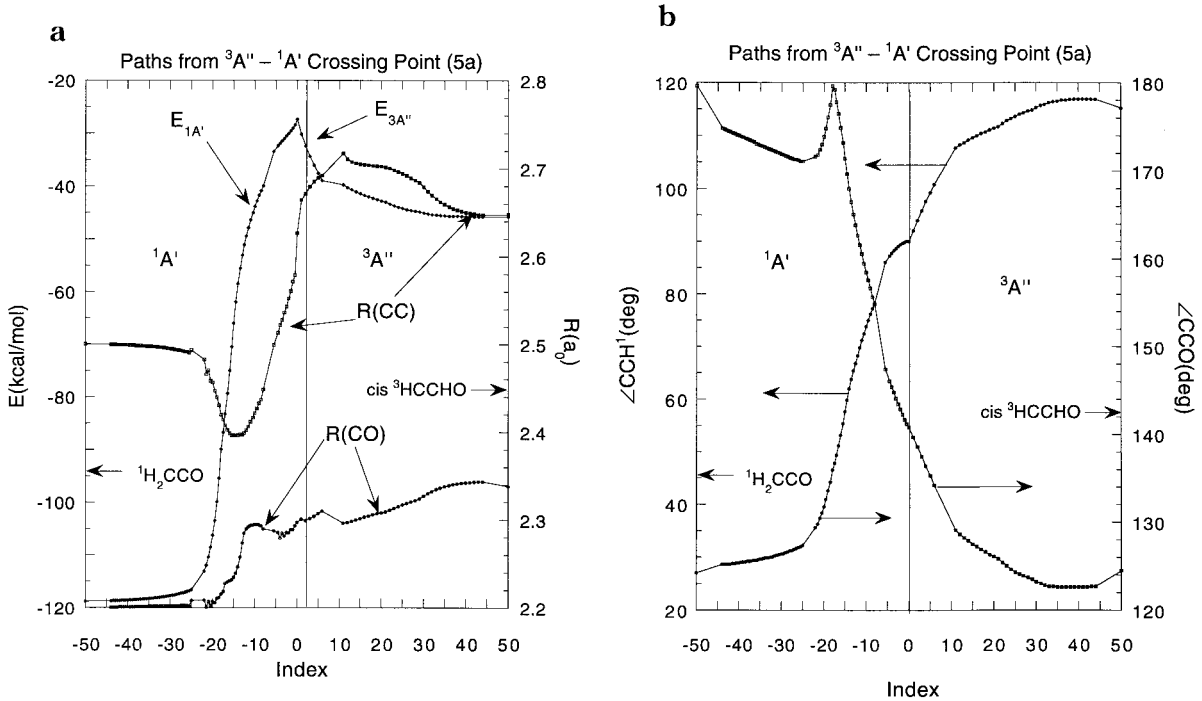

Figure 4. Gradient directed paths on $^3A''$ and $^1A'$ potential energy surfaces from point *5a* of Table 1. For each step taken on the gradient directed path on the $^3A''$ ($^1A'$) potential energy surface Index was incremented by 1 (−0.5). Index = 0 at point *5a*. A small *local* barrier (<4 kcal/mol) not well described by this procedure exists between points +5 and +10. No such barrier is observed from point *5b*. 4(a) Energy, R(C−C) and R(C^1−O); (b) ∠CCO, ∠CCH^1, and ∠H^{2}CC.

configuration can correlate smoothly with $H_2CCO(\tilde{X}^1A_1)$, consistent with the absence of a barrier on the $^1A'$ surface to $H_2CCO(\tilde{X}^1A_1)$ from the points of intersection described above. The $^3A''$ state is dominated by the $C_I[^3A'']$ so that $H^{so}(^3A') \approx \langle 2a''|h_{eff}^{so}|10a'\rangle$. The $2a''$ orbital is an antibonding mixture of a″(1) + a″(2) and a″(3). Similarly, $10a'$ is a mixture of a′(1) and a′(2). The geometry dependence of the atomic orbital contributions to the molecular orbitals produces the large differences in $H^{so}(^3A'')$ observed for points *5a* and *5b*. In future work, it will be important to examine the effect on $H^{so}(^3A'')$ of modifying the active space as described in section II.

E. Mechanistic Implications. There has been considerable interest in the branching ratio for the production of $^3CH_2$ and $^1CH_2$ from the reaction of $O(^3P)$ with acetylene. The calculations reported herein provide a valuable guide to the factors that must be considered to model this branching. Our calculations indicate the need to consider efficient internal conversion of the 2^3A state to the 1^3A state driven by $^3A'-^3A''$ conical intersections. On the $^3A''$ potential energy surface, the intermediate complex $^3HCCHO(^3A'')$ provides for repeated access to low energy, but spin-forbidden, pathways to $CH_2(\tilde{a}^1A_1)$. The key to describing these pathways is the intersystem crossing/isomerization $^3HCCHO \rightarrow {}^1H_2CCO$ for which $\angle C^2C^1H^1$ can be taken as an approximate reaction coordinate. The calculations reported here present data on the possiblility of intersystem crossing at three values of $\angle C^2C^1H^1$: ∼117° (the ketocarbene region), 90°, and ∼64° (TS2). In each case, energetically accessible singlet−triplet intersections−that is intersections at energies lower than TS1″ (Figure 1)−were found. Thus, we have the interesting situation where intersystem crossing is possible *continuously* in the vicinity of the path from ^3HCCHO to TS2. This intersystem crossing provides, except for the immediate region of the ketocarbene complexes, virtually barrierless pathways to ^1H_2CCO-like structures. In the ketocarbene region, we find that, at least for some crossing points, the gradient-directed paths on the $^1A'$ potential energy surface lead to a planar local minimum with a HCCHO structure. When the constraint of planarity is relaxed for these points, direct paths to ^1H_2CCO were not found using the gradient-directed path method. However, intersystem crossing in this region can still lead to singlet products provided energy redistribution takes the system to the products before recrossing to the triplet surface can occur.

The preceding analysis evinces the key role intramolecular energy redistribution plays in determining the $^3CH_2/^1CH_2$ branching ratio. Funneling energy into modes perpendicular to the reaction coordinate favors production of $^1CH_2$ by increasing the lifetime of the complex and reducing the velocity in the direction of the energy difference gradient. It is hoped that the present results will stimulate modeling of this process.

It is known that in larger alkynes when $CO(X^1\Sigma^+)$ is produced, the channel leading to the singlet carbene, the spin-forbidden channel, is preeminent. The present analysis suggests two possible explanations for this result: (i) the increased number of internal modes increases the lifetime of the intermediate complex favoring intersystem crossing or (ii) the barrier on the triplet surface separating the ketocarbene and the substituted ketene increases inhibiting the spin-allowed channel. In future work, we hope to address the later hypothesis.

IV. Summary and Conclusions

The mechanism of the spin-forbidden reaction 1b is discussed. Portions of the $^3A''-{}^1A'$, $^3A'-{}^1A'$, and 1^3A-2^3A surfaces of intersection and spin−orbit coupling matrix elements were determined using multireference configuration interaction wave functions comprised of 330 000−1 100 000 CSFs. The key result is that intersystem crossing can take place continuously as H migrates uphill from ^3HCCHO to the $^3HCCHO \rightarrow {}^3H_2CCO$ transition state. This region is exoergic relative to the $O(^3P)$ + HCCH reactants.

Acknowledgment. D.R.Y. was supported in part by DOE-BES Grant DE-FG02-91ER14189. The calculations reported in this work were performed on D.R.Y.'s IBM RS 6000 workstations purchased with funds provided by AFOSR, DOE, and NSF grants.

References and Notes

(1) Yarkony, D. R. *Int. Reviews of Phys. Chem.* **1992**, *11*, 195−242.
(2) DeMore, W. B.; Raper, O. F. *J. Chem. Phys.* **1962**, *37*, 2048.
(3) Tully, J. C. *J. Chem. Phys.* **1974**, *61*, 61.
(4) Zahr, G. E.; Preston, R. K.; Miller, W. H. *J. Chem. Phys.* **1975**, *62*, 1127−1135.
(5) Harding, L. B.; Wagner, A. F. *J. Phys. Chem.* **1986**, *90*, 2974−2987.
(6) Schmoltner, A. M.; Chu, P. M.; Lee, Y. T. *J. Chem. Phys.* **1990**, *91*, 5365−5372.
(7) Huang, X.; Xing, G.; Bersohn, R. *J. Chem. Phys* **1994**, *101*, 5818.
(8) Huang, X.; Xing, G.; Wang, X.; Bersohn, R. *J. Chem. Phys* **1996**, *105*, 488−495.
(9) Hucknall, D. J. *Chemistry of Hydrocarbon Combustion*; Chapman and Hall: New York, 1985.
(10) Allen, W. D.; Schaefer, H. F., III. *J. Chem. Phys.* **1988**, *89*, 329−344.
(11) Klippenstein, S. J.; East, A. L. L.; Allen, W. D. *J. Chem. Phys* **1996**, *105*, 118−140.
(12) Bargon, K.; Tanaka, K.; Yoshimine, M. Computer Chemistry Studies of Organic Reactions: The Wolff Rearrangement. In *Computational Methods in Chemistry*; Bargn, J., Ed.; Plenum: New York, 1980; pp 239−274.
(13) Lengsfield, B. H.; Yarkony, D. R. *Nonadiabatic Interactions Between Potential Energy Surfaces: Theory and Applications.* In *State-Selected and State to State Ion−Molecule Reaction Dynamics: Part 2 Theory*; Baer, M., Ng, C.-Y., Eds.; John Wiley & Sons: New York, 1992; Vol. 82, pp 1−71.
(14) Shavitt, I. The Method of Configuration Interaction. In *Modern Theoretical Chemistry*; Schaefer, H. F., Ed.; Plenum Press: New York, 1976; Vol. 3, p 189.
(15) Roos, B. O. *Int. J. Quantum Chem. Symp*. **1980**, *14*, 175.
(16) Roos, B. O.; Taylor, P. R.; Siegbahn, P. E. M. *Chem. Phys.* **1980**, *48*, 157.
(17) Siegbahn, P.; Heiberg, A.; Roos, B.; Levy, B. *Phys. Scr.* **1980**, *21*, 323.
(18) Dunning, T. H. *J. Chem. Phys.* **1971**, *55*, 716.
(19) Yarkony, D. R. Electronic Structure Aspects of Nonadiabatic Processes in Polyatomic Systems. In *Modern Electronic Structure Theory*; Yarkony, D. R., Ed.; World Scientific: Singapore, 1995; pp 642−721.
(20) Truhlar, D. G.; Mead, C. A.; Brandt, M. A. *Adv. Chem. Phys.* **1975**, *33*, 295.
(21) Mead, C. A. *J. Chem. Phys.* **1979**, *70*, 2276.
(22) Moore, C. E. *Atomic Energy Levels, Natl. Stand. Ref. Data Ser., Natl. Bur. Stand.*; U. S. GPO: Washington, DC, 1971; Vol. 3.
(23) East, A. L. L.; Allen, W. D.; Klippenstein, S. J. *J. Chem. Phys.* **1995**, *102*, 8506.
(24) Fukui, K. *Acc. Chem. Res.* **1981**, *14*, 363.